Focusing and Impedance Properties of Conformable Phased Array Antennas for Microwave Hyperthermia

Reza M. Najafabadi and Andrew F. Peterson, *Senior Member, IEEE*

Abstract—**Phased array applicators for microwave hyperthermia are usually developed using planar, layered tissue models, and then evaluated using numerical techniques. The present investigation considers the use of a cylindrical, layered tissue model to replace the first step of the design procedure. This model facilitates an evaluation of the impact of curvature, polarization, and bolus materials on the antenna performance.**

I. Introduction

OVER THE past two decades, antennas used for noninvasive hyperthermia have evolved from single-element applicators such as dielectric-loaded horn antennas to phased array applicators capable of considerable control over the heating pattern [1]–[3]. Phased arrays offer several advantages compared with single-element applicators. In addition to real-time dynamic control, phased arrays offer the possibility of focusing the energy at the tumor location, providing deeper energy penetration into the biological tissue, and reducing the undesired surface heating associated with a hyperthermia treatment. Existing designs are generally planar and have been developed based on tissue models that are homogeneous or layered [1]–[3].

In the present investigation, we consider conformable phased array applicators. These applicators radiate into an environment consisting of a bolus layer used for cooling, followed by layers of skin, fat, and muscle tissue, which in general may be nonuniform and heterogeneous. Consequently, the actual tissue environment is complex. For analysis purposes, the heterogeneous tissue environment is best treated with a high resolution numerical technique, such as finite elements [4] or the finite-difference time-domain (FDTD) approach [5]. However, early in the design process it is advantageous to work with a simpler model incorporating the coarse features of the tissue geometry. One possible model consists of a cylindrically layered region of dielectric material, illuminated by aperture sources in a conducting circular cylinder that surrounds the tissue as in Fig. 1. Any number of apertures may be excited with arbitrary amplitude and phase in order to achieve a desired focusing effect. Because of the lossy characteristics of fat and muscle tissue, the signal produced by the aperture sources will decay to insignificant levels before reaching the opposite side of the circular conducting cylinder.

Manuscript received November 15, 1995; revised April 2, 1996. This work was supported in part by the National Science Foundation under Grant ECS-9257927.

The authors are with the School of Electrical and Computer Engineering, Georgia Institute of Technology, Atlanta, GA 30332-0250 USA.

Publisher Item Identifier S 0018-9480(96)07026-3.

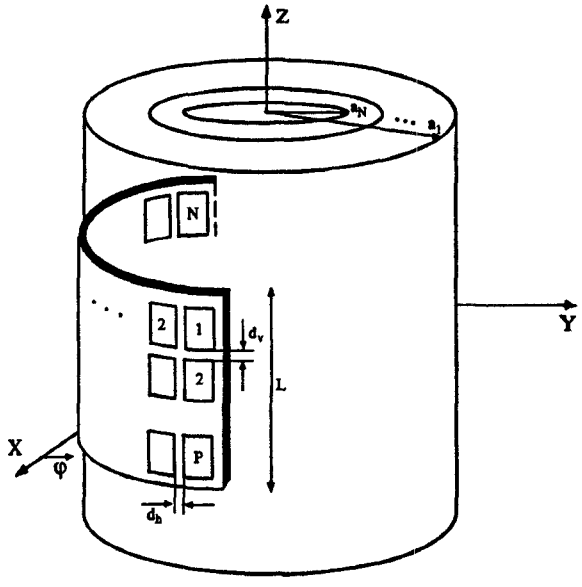

Fig. 1. The geometry of the cylindrical conformable antenna and tissue model. The antenna consists of N apertures in a two-dimensional (2-D) configuration for focusing. A bolus region has been placed between the antenna and the tissue surface.

Thus, the model is intended to mimic the near-zone region immediately in front of the actual cylindrical applicator, and can be used to study parameters associated with the curvature of the ground plane, the materials comprising the tissue layers, or the degree of focusing possible.

The two major approximations associated with this model are that 1) the actual tissue environment will not be cylindrical and 2) the mutual coupling between the aperture radiators will be ignored. These assumptions are a necessary feature of the model, since neither approximation can be improved upon without resorting to numerical analysis to solve the actual electromagnetics problem. Thus, while the model will be a useful tool for comparing various antenna designs, it is not intended to replace a more rigorous analysis of an actual hyperthermia treatment scenario.

II. Mathematical Model

Consider an infinite length perfectly conducting circular cylinder with multiple apertures on its surface as shown in Fig. 1. The interior region contains inhomogeneous material modeled as N concentric layers with radius a_n, where $n = 1, \cdots N$; a_1 is the radius of the most exterior cylinder and a_N is the radius of the most interior cylinder. Each layer

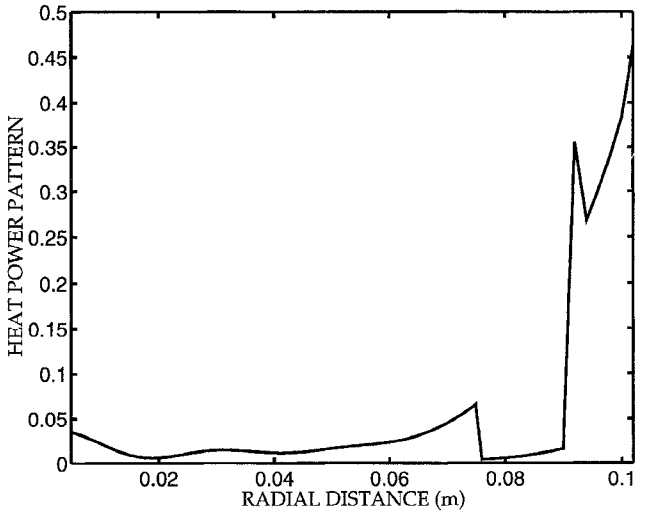

Fig. 2. The power pattern produced by a 3 × 7 phased array antenna with axially polarized electric field apertures. A bolus of 1.0 cm thickness with $\epsilon = 14$ and $\sigma = 0.85$ [S/m] has been used. The overall array dimensions are 15.7 cm (axial dimension) × 18.5 cm (circumferential dimension).

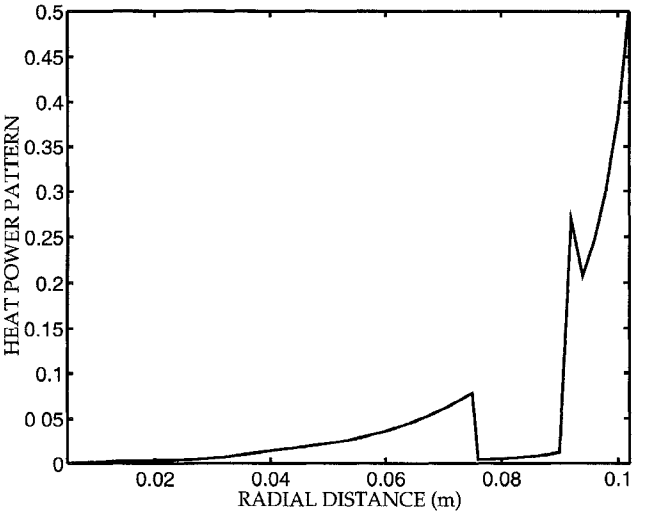

Fig. 4. The power pattern produced by a 7 × 3 phased array antenna with circumferentially polarized elements. A bolus of 1.0 cm thickness with $\epsilon = 14$ and $\sigma = 0.85$ [S/m] has been used. The overall array dimensions are 16 cm (axial dimension) × 13 cm circumferential dimension).

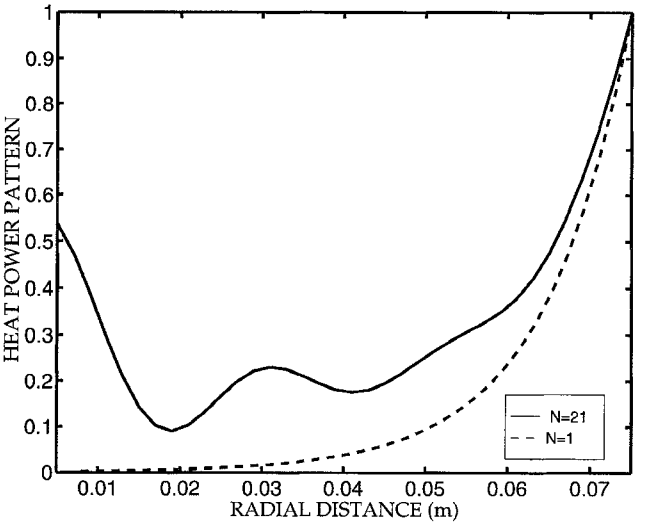

Fig. 3. Comparison between the power pattern in the muscle region for a single aperture and a 3 × 7 phased array of the same overall dimension. Both cases use a bolus of 1.0 cm thickness with $\epsilon = 14$ and $\sigma = 0.85$ [S/m].

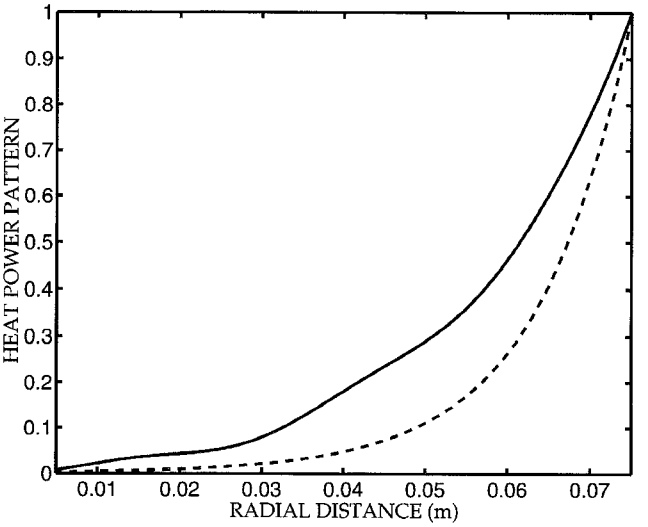

Fig. 5. Comparison between the power pattern in the muscle region for a single element array and a 7 × 3 phased array. Both cases use a bolus of 1.0 cm thickness with $\epsilon = 14$ and $\sigma = 0.85$ [S/m].

n is characterized by a permittivity ϵ_n and conductivity σ_n. The magnetic permeability of the entire system is assumed to be μ_0. The electromagnetic fields are described in (ρ, φ, z) cylindrical coordinates. The electromagnetic field components can be determined by the solution of the Helmholtz wave equation, which produces electric fields in layer n that can be written [6] as

$$E_z(\rho, \varphi, z) = \int_{-\infty}^{+\infty} \sum_{m=-\infty}^{+\infty} [-\nu_n^2 K_m(\nu_n\rho) A_m^n - \nu_n^2 I_m(\nu_n\rho) C_m^n] e^{-jm\varphi} e^{-j\lambda z}\, d\lambda \quad (1)$$

$$E_\varphi(\rho, \varphi, z) = \int_{-\infty}^{+\infty} \sum_{m=-\infty}^{+\infty} \frac{-m\lambda}{\rho} [A_m^n K_m(\nu_n\rho) + C_m^n I_m(\nu_n\rho)] e^{-jm\varphi} e^{-j\lambda z}\, d\lambda + \int_{-\infty}^{+\infty} \sum_{m=-\infty}^{+\infty} j\omega\mu_n\nu_n [B_m^n K_m'(\nu_n\rho) + D_m^n I_m'(\nu_n\rho)] e^{-jm\varphi} e^{-j\lambda z}\, d\lambda \quad (2)$$

$$E_\rho(\rho, \varphi, z) = \int_{-\infty}^{+\infty} \sum_{m=-\infty}^{+\infty} -j\lambda\nu_n [A_m^n K_m'(\nu_n\rho) + C_m^n I_m'(\nu_n\rho)] e^{-jm\varphi} e^{-j\lambda z}\, d\lambda + \int_{-\infty}^{+\infty} \sum_{m=-\infty}^{+\infty} -\frac{m\omega\mu_n}{\rho} [B_m^n K_m(\nu_n\rho) + D_m^n I_m(\nu_n\rho)] e^{-jm\varphi} e^{-j\lambda z}\, d\lambda \quad (3)$$

where ν_n is given by $\nu_n^2 = \lambda^2 + \gamma_n^2$ with $\mathrm{Re}\,(\nu_n) > 0$, and $\gamma^2 = j\omega\mu(\sigma + j\omega\epsilon)$ for each layer. $I_m(\nu\rho)$ and $K_m(\nu\rho)$ are modified Bessel functions with argument $\nu_n\rho$ and order

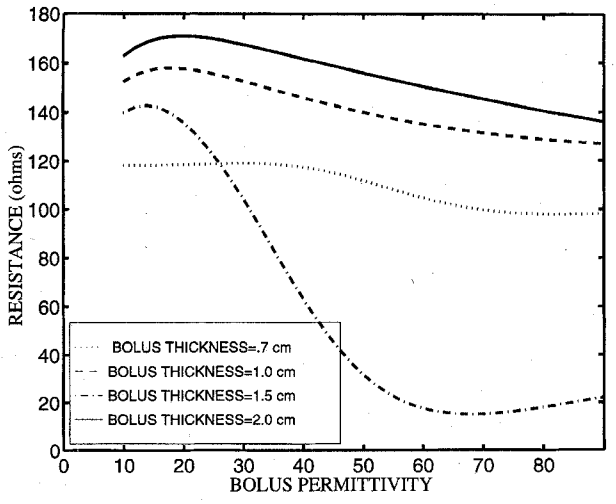

Fig. 6. The resistive part of the wave impedance at the tissue surface versus the bolus permittivity for bolus conductivity $\sigma = 0.55$ [S/m].

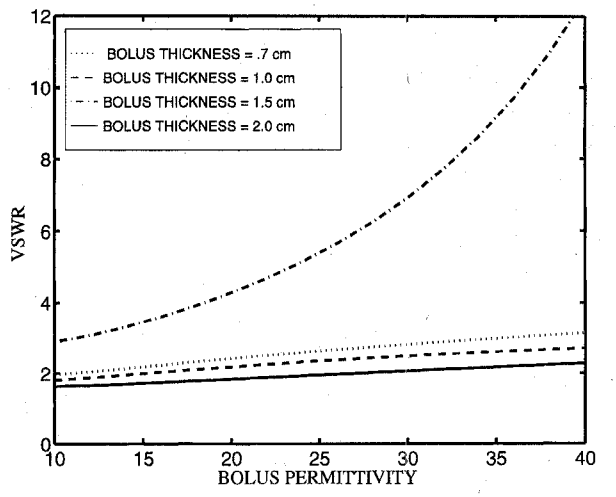

Fig. 8. The standing wave ratio in the bolus region versus the bolus permittivity for different bolus thicknesses and bolus conductivity of 0.55 [S/m].

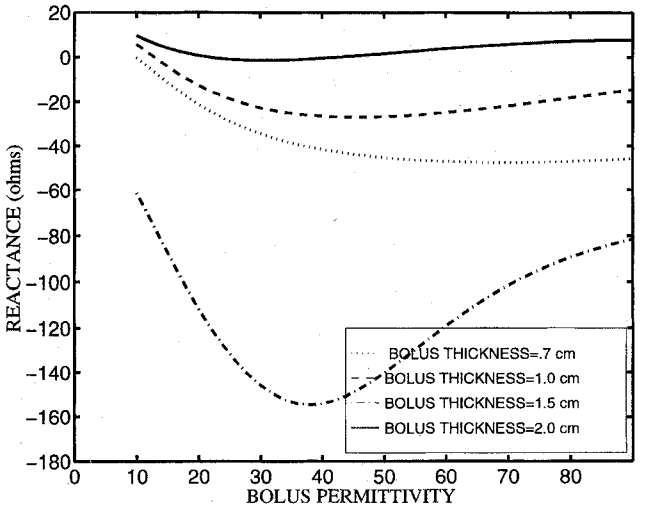

Fig. 7. The reactive part of the wave impedance at the tissue surface versus the bolus permittivity for bolus conductivity $\sigma = 0.55$ [S/m]. The aperture has an axial length of 2.5 cm and circumferential length of 5.0 cm.

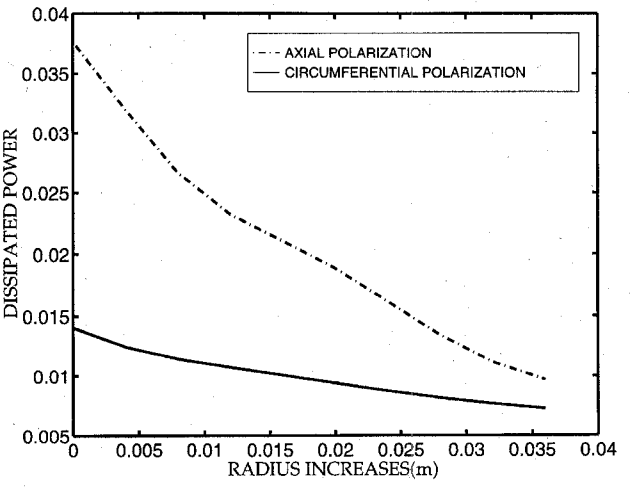

Fig. 9. An illustration of the effect of the antenna curvature on the power produced at $\rho = 5.0$ cm for the axial and circumferential polarizations, as the radius of the cylinder increases from 10.2–14.2 cm.

m. A_m^n, B_m^n, C_m^n, and D_m^n are coefficients to be determined. These coefficients can be determined by enforcing continuity of tangential fields at the interface between any two layers and at the apertures. After the values of the electromagnetic fields on boundary layer n are expressed in terms of the values on layer one, the coefficients can be determined from

$$\begin{bmatrix} A_m^n \\ B_m^n \\ C_m^n \\ D_m^n \end{bmatrix} = [P_m^n(a_n)]^{-1} \begin{bmatrix} E_{z_m}(\rho) \\ H_{z_m}(\rho) \\ E_{\varphi_m}(\rho) \\ H_{\varphi_m}(\rho) \end{bmatrix} \tag{4}$$

where $[P_m^n(a_n)]$ is given by (5), as shown at the bottom of the page, and I'_m and K'_m are the derivative of the modified Bessel functions with respect to $(\nu_n\rho)$. To evaluate (1)–(3) numerically one must truncate the summation and the integral at finite values. This procedure is assisted by determining the symmetry properties of the integrands and summations, as described in [6].

The equivalence of the closed mathematical cylinder and the open, curved applicators can be established by demonstrating that the fields decay to insignificant levels beyond the extent of the curved applicator. This was demonstrated for each of

$$[P_m^n(\rho)] = \begin{bmatrix} -\nu_n^2 K_m(\nu_n\rho) & 0 & -\nu_n^2 I_m(\nu_n\rho) & 0 \\ 0 & -\nu_n^2 K_m(\nu_n\rho) & 0 & -\nu_n^2 I_m(\nu_n\rho) \\ -\dfrac{m\lambda}{\rho} K_m(\nu_n\rho) & j\omega\mu_n\nu_n K'_m(\nu_n\rho) & -\dfrac{m\lambda}{\rho} I_m(\nu_n\rho) & j\omega\mu_n\nu_n I'_m(\nu_n\rho) \\ -\hat{\sigma}_n\nu_n K'_m(\nu_n\rho) & -\dfrac{m\lambda}{\rho} K_m(\nu_n\rho) & -\hat{\sigma}_n\nu_n I'_m(\nu_n\rho) & -\dfrac{m\lambda}{\rho} I_m(\nu_n\rho) \end{bmatrix} \tag{5}$$

the simulations to follow [6]. In addition, the formulation and numerical implementation was verified by comparing with the 2-D results of Wait and Lumori [7], and the three-dimensional (3-D) results of Ho [8]. The results are identical as far as can be determined from the published figures. At 915 MHz, the frequency used in the following simulation, we use $\epsilon_r = 51$ and $\sigma = 1.28$ [S/m] for skin and muscle, and $\epsilon_r = 5.6$ and $\sigma = 0.066$ [S/m] for fat.

III. Focusing Properties of the Curved Array

To demonstrate the focusing properties of the curved array applicators, Figs. 2 and 3 show the power deposition pattern for a geometry consisting of an inner cylinder of muscle tissue (radius 7.5 cm) surrounded by a 1.5 cm layer of fat, a 2 mm layer of skin, and a bolus layer of thickness 1 cm, $\sigma = 0.85$ [S/m] and $\epsilon_r = 14$. The source is a 3×7 array occupying a 15.7 cm $\times$ 18.5 cm region; and phased to focus at a depth of 5.2 cm (location $\rho = 0.05$ m), for the axial polarization. Fig. 3 also shows the power pattern for a single aperture. Fig. 2 shows the power density as a function of the radial distance; the region $0 < \rho < 0.075$ corresponds to muscle tissue, $0.075 < \rho < 0.09$ to fat, $0.09 < \rho < 0.092$ to skin, and $0.092 < \rho < 0.102$ to bolus, with the array apertures located at $\rho = 0.102$ m. In Fig. 3, only the muscle region is shown and the power density is normalized at the muscle surface. Figs. 4 and 5 show similar results for an array of 7×3 apertures of dimensions 16.0 cm $\times$ 13.0 cm, for the circumferential polarization (E_φ excitation). Figs. 3 and 5 show that the axial polarization is more successful in focusing the fields. Despite losses in the bolus layer and tissue regions, the array antenna can partially focus the energy. Although physiological constraints severely limit the focusing of microwave energy in tissue, these simulations suggest that some focusing is possible and that the axial polarization is better suited for focusing in the cylindrical array configuration.

IV. Use of Bolus Layer to Enhance the Impedance Match

The material and thickness of the bolus layer introduce degrees of freedom that can be used to improve the applicator performance. In the present investigation, we varied these parameters to determine their effect on the wave impedance (the ratio of tangential electric to tangential magnetic field) seen "looking into" the lossy cylinder comprising the tissue. Figs. 6–8 show the fluctuation in the wave impedance as a function of the bolus permittivity and thickness. The large fluctuations suggest that the bolus can in fact be used to enhance the impedance match between the applicator and the tissue. In general, the fluctuations as a function of permittivity were far more severe than the fluctuations as a function of conductivity, so only permittivity plots are included. For a bolus thickness of 0.7 cm, the presence of a large standing wave between the applicator and tissue increases the sensitivity of the system to slight change in materials, thickness of layers, etc. By an appropriate choice of bolus material and thickness, the standing wave between the applicator and target region can be minimized and the sensitivity reduced.

V. Impact of Curvature

One of the primary reasons for developing the curved applicator model is to study the effect of ground-plane curvature on the array pattern and other properties. Fig. 9 illustrates this by showing the power delivered to a focal point as the radius of the model is varied. The tissue model contains 1.5 cm fat, 2.0 mm skin, and uses a 1.0 cm bolus layer, while the muscle thickness is varied from 7.5–11.5 cm. Again, it appears that the axial polarization is generally more effective than the circumferential at delivering power to the tissue.

VI. Conclusion

The design of hyperthermia applicators can be enhanced by the early incorporation of parameters such as ground plane curvature, bolus material, and thickness into the preliminary design process. A cylindrically layered tissue model was studied and confirms that these parameters can have a substantial impact on applicator performance.

References

[1] W. Gee, S. W. Lee, N. K. Bong, C. A. Cain, R. Mittra, and R. L. Magin, "Focused array hyperthermia applicator: Theory and experiment," *IEEE Trans. Biomed. Eng.*, vol. BME-31, pp 38–46, Jan. 1984

[2] J. W. Hand, J. L. Cheetham, and A. J. Hind, "Absorbed power distributions from coherent microwave arrays for localized hyperthermia," *IEEE Trans. Microwave Theory Tech.*, vol. MTT-34, pp. 484–488, 1986.

[3] R. L. Magin and A. F. Peterson, "Non-invasive microwave phased arrays for local hyperthermia. A review," *Int. J Hyperthermia,* vol 5, pp 429–450, 1989.

[4] D R. Lynch, K. D. Paulsen, and J. W. Strohbehn, "Hybrid element method for unbounded electromagnetic problems in hyperthermia," *Int. J. Numerical Methods Engineering,* vol. 23, pp. 1915–1937, 1986.

[5] D. M. Sullivan, D. T. Borup, and O. P. Gandhi, "Use of the finite-difference time-domain method in calculating EM absorption in human tissues," *IEEE Trans. Biomed. Eng* , vol. 34, pp. 148–157, Feb. 1987.

[6] R M Najafabadi, "Analysis and design of cylindrically conformable microwave phased array antennas for hyperthermia applications," Ph.D. dissertation, Georgia Inst. Technol., Atlanta, GA, May 1995.

[7] J. R. Wait and M. L. D. Lumori, "Focused heating in cylindrical targets. II," *IEEE Trans. Microwave Theory Tech.*, vol MTT-34, pp. 357–359, Mar. 1986.

[8] H. S. Ho, "Microwave heating of simulated human limbs by aperture sources," *IEEE Trans. Microwave Theory Tech.*, vol. MTT-19, pp. 224–231, Feb. 1971.

Reza M. Najafabadi received the B.E.E. degree from Shiraz University of Science and Technology, Tehran, Iran, in 1980 and the M.S.E.E. and Ph.D. degrees in electrical engineering from the Georgia Institute of Technology, Atlanta, in 1992 and 1995, respectively. He also received the M.S. degree in applied mathematics from Georgia Tech in 1994.

He is currently employed by the Wang Electro-Opto Corporation, Marietta, GA.

Andrew F. Peterson (S'82–M'83–SM'92), for a photograph and biography, see p. 879 of the June 1996 issue of this TRANSACTIONS